

# Inelastic Dark Matter at the LHC

Yang Bai<sup>a</sup> and Tim M.P. Tait<sup>b</sup>

<sup>a</sup>SLAC National Accelerator Laboratory, 2575 Sand Hill Road, Menlo Park, CA 94025, USA,

<sup>b</sup>Department of Physics and Astronomy, University of California, Irvine, CA 92697, USA

We perform a model-independent study of inelastic dark matter at the LHC, concentrating on the parameter space with the mass splitting between the excited and ground states of dark matter above a few hundred MeV, where the direct detection experiments are unlikely to explore. The generic signatures of inelastic dark matter at the LHC are displaced pions together with a monojet plus missing energy, and can be tested at the 7 TeV LHC.

PACS numbers: 12.60.-i, 95.35.+d, 14.80.-j

**Introduction.** Despite overwhelming evidence from astrophysical observation, we still don't know the particle properties of dark matter (DM) or how it interacts with standard model (SM) particles. Dark matter as a weakly interacting massive particle (WIMP) is predicted in many extensions of the SM and motivates searches for its direct detection, where one looks for ambient WIMPs scattering with heavy nuclei. An implicit assumption in these searches is that DM particles can scatter elastically off detector nuclei. So far, there are no unambiguous signals for a detection of DM scattering, leading to strong bounds on WIMPs with weak scale interactions [1].

These null results raise severe questions about the viability of the WIMP paradigm, and motivate theoretical exploration of modifications of the standard picture. For example, if dark matter is required to scatter inelastically into a state heavier than the initial WIMP by  $\gtrsim 1$  MeV, typical WIMPs in the Milky Way halo will have insufficient energy to upscatter, explaining the null results of direct detection experiments. Nonetheless, we shall see below that inelastic dark matter (iDM) models can be tested at the Large Hadron Collider (LHC). The iDM models were introduced some time ago [2, 3] to evade constraints on models from null DM direct detection searches, and were recently revisited to reconcile the DAMA observation of annual modulation [4] with other null direct searches [5], provided the mass splitting is below a few hundred keV.

In this letter, we explore the LHC's capability to identify iDM scenarios through a model-independent, effective field theory (EFT) approach [6–10]. We discuss general strategies and characterize signatures appropriate for different parameter space. The mass splitting  $\Delta$  and coefficients of the various EFT operators control the lifetime of the excited DM particle, but it is generically long-lived on collider time scales. If the mass splitting is too small, the decay products of the excited state are too soft to be observed and the generic signature is a monojet plus missing energy [7–9]. However, for mass splittings  $\gtrsim 1$  GeV, iDM results in a spectacular signature with displaced pions appearing on top of the monojet signature.

**Operators and interactions.** We assume the dark sector is composed of two SM gauge singlet fermions  $\chi$

and  $\chi_*$  with masses  $m$  and  $m_*$ , where  $\Delta \equiv m_* - m > 0$  characterizes the splitting between the two states. We assume that interactions with the SM are required to contain one  $\chi$  and  $\chi_*$  each, and (for simplicity) restrict ourselves to interactions consisting of operators which involve the up-quark and preserve parity:

$$\begin{aligned} \mathcal{O}_1 &= \frac{[\bar{u} \gamma_\mu \gamma_5 u] [\bar{\chi}_* \gamma^\mu \gamma_5 \chi]}{\Lambda_1^2}, & \mathcal{O}_2 &= \frac{[\bar{u} \gamma_5 u] [\bar{\chi}_* \gamma_5 \chi]}{\Lambda_2^2}, \\ \mathcal{O}_3 &= \frac{[\bar{u} u] [\bar{\chi}_* \chi]}{\Lambda_3^2}, & \mathcal{O}_4 &= \frac{[\bar{u} \gamma_\mu u] [\bar{\chi}_* \gamma^\mu \chi]}{\Lambda_4^2}. \end{aligned} \quad (1)$$

where  $\Lambda_i$  parameterizes the strength of each interaction. The effective Lagrangian consists of the SM plus kinetic terms for  $\chi$  and  $\chi_*$ , as well as these operators plus their complex conjugates.

We are interested in mass splittings ranging from 100 MeV to several GeV. For  $\Delta \lesssim 1$  GeV, we can use the chiral Lagrangian to describe how these interactions lead to  $\chi_*$  decaying into  $\chi$  plus a number of pions. We focus on non-vanishing terms with the minimum number of pion legs, since higher order interactions are phase-space suppressed. The leading terms for each operator are

$$\begin{aligned} \mathcal{O}_1 &\rightarrow \frac{F_\pi}{2\Lambda_1^2} [\bar{\chi}_* \gamma_5 \gamma^\mu \chi] (\partial_\mu \pi^0), \\ \mathcal{O}_2 &\rightarrow \frac{i \langle \bar{u} u \rangle}{F_\pi \Lambda_2^2} [\bar{\chi}_* \gamma_5 \chi] \pi^0, \\ \mathcal{O}_3 &\rightarrow -\frac{\langle \bar{u} u \rangle}{2F_\pi^2 \Lambda_3^2} [\bar{\chi}_* \chi] (\pi^0 \pi^0 + 2\pi^+ \pi^-), \\ \mathcal{O}_4 &\rightarrow \frac{1}{\Lambda_4^2} [\bar{\chi}_* \gamma^\mu \chi] (\pi^- \partial_\mu \pi^+ - \pi^+ \partial_\mu \pi^-), \end{aligned} \quad (2)$$

where  $F_\pi = 184$  MeV and  $\langle \bar{u} u \rangle = -(242 \text{ MeV})^3$  (evaluated at 1 GeV) [11]). For on-shell  $\chi$  and  $\chi_*$ ,  $\mathcal{O}_1$  can be rewritten in terms of  $m$  and  $m_*$ , in analogy with the usual treatment of pion-nucleon interactions. The parity of the quark bilinears involved dictate that the leading terms induced by  $\mathcal{O}_{1,2}$  in the chiral Lagrangian correspond to one pion interactions, whereas  $\mathcal{O}_{3,4}$  correspond to interactions involving at least two pions. For theories in which dark matter also couples to down-quarks, the right-hand side of Eq. (2) for  $\mathcal{O}_{1,4}$  project onto the iso-

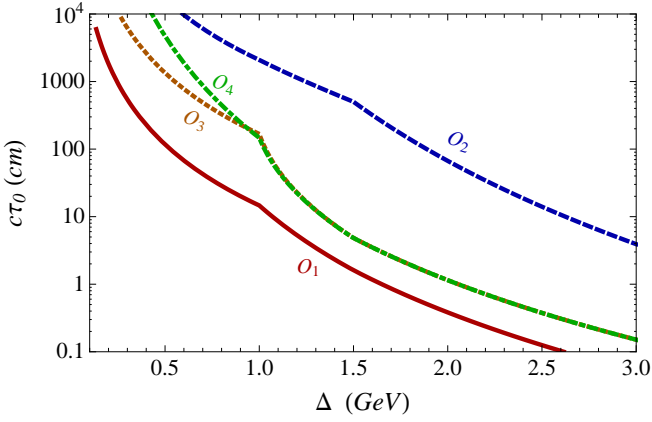


FIG. 1: Decay lengths of the excited dark matter state at rest as a function of mass splitting for different operators with  $\Lambda_i = 1$  TeV and a dark matter mass of 5 GeV.

spin violating terms, whereas for  $\mathcal{O}_{2,3}$  arise from iso-spin conserving pieces.

**Decay of the  $\chi_*$ .** We concentrate on the regions of parameter space with  $\Delta \geq m_{\pi^0}$  (for  $\mathcal{O}_{1,2}$ ) or  $\Delta \geq 2m_{\pi^+}$  (for  $\mathcal{O}_{3,4}$ ), for which decays lead to real pions and result in hard enough decay products so as to register in LHC detectors. We deal with the regimes  $\Delta \lesssim 1$  GeV (described by the chiral Lagrangian) and  $\Delta \gtrsim 1.5$  GeV (described by interactions with quarks) separately.

For  $\Delta \lesssim 1$  GeV,  $\mathcal{O}_1$  and  $\mathcal{O}_2$ , lead to two-body decays  $\chi_* \rightarrow \chi + \pi^0$  with decay widths  $\Gamma_i$  ( $i=1,2$ )

$$\alpha_i^2 \frac{(\Delta^2 - m_{\pi^0}^2) \sqrt{(\Delta^2 - m_{\pi^0}^2)(4\bar{m}^2 - m_{\pi^0}^2)}}{16\pi m_*^3}, \quad (3)$$

where  $\bar{m} \equiv (m_* + m)/2$ ,  $\alpha_1 = F_\pi \bar{m}/\Lambda_1^2$ , and  $\alpha_2 = |\langle \bar{u}u \rangle|/(F_\pi \Lambda_2^2)$ . In the limit  $\bar{m} \gg \Delta > m_{\pi^0}$ ,  $\Gamma_1$  is roughly independent of the DM mass, and  $\Gamma_2 \propto \Delta^3/\bar{m}^2$ . Operators  $\mathcal{O}_{3,4}$  result in three-body decays of  $\chi_*$  to  $\chi$  plus two pions. Neglecting pion masses and in the limit  $\bar{m} \gg \Delta$ ,

$$\Gamma_3(\chi_* \rightarrow \chi \pi^+ \pi^-) = 2\Gamma_3(\chi_* \rightarrow \chi \pi^0 \pi^0) = \frac{\langle \bar{u}u \rangle^2 \Delta^3}{48\pi^3 F_\pi^4 \Lambda_3^4},$$

$$\Gamma_4(\chi_* \rightarrow \chi \pi^+ \pi^-) = \frac{\Delta^5}{240\pi^3 \Lambda_4^4}. \quad (4)$$

For  $\Delta \gtrsim 1.5$  GeV, the chiral Lagrangian is no longer a suitable description, and we compute  $\chi_* \rightarrow \chi q \bar{q}$ ,

$$\Gamma(\chi_* \rightarrow \chi u \bar{u}) = \frac{a_i \Delta^5}{\pi^3 \Lambda_i^4}, \quad (5)$$

where  $a_1 = 1/20$ ,  $a_2 = \Delta^2/(560\bar{m}^2)$ , and  $a_3 = a_4 = 1/60$ . The decay produces soft jets of hadrons (mostly pions with a small fraction of kaons) described by the parton shower of QCD. The intermediate region of  $1 \text{ GeV} \lesssim \Delta \lesssim 1.5 \text{ GeV}$  is complicated, and receives contributions from resonances as well as multi-pion states.

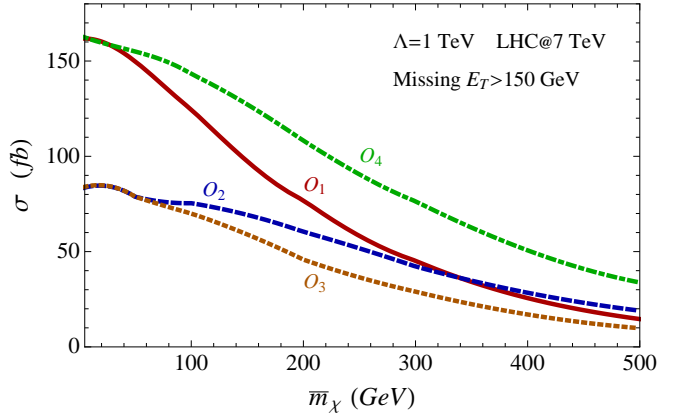


FIG. 2: Production cross section of  $pp \rightarrow \chi_e \bar{\chi}_g j$  at the 7 TeV LHC.

We have approximated the behavior in this region by requiring the decay length smoothly interpolate between the leading decay for small  $\Delta$  and the soft jet regime of large  $\Delta$ .

Decay lengths  $c\tau_0$  as a function of  $\Delta$ , for  $\Lambda_i = 1$  TeV and  $\bar{m} = 5$  GeV are shown in Fig. 1. Different values of  $\Lambda_i$  rescale the presented lifetime by  $(\Lambda_{\text{new}}/1 \text{ TeV})^4$ . For the chosen parameters, they vary from 1 cm to 10 m, depending on  $\Delta$  and the operator mediating the decay. As we shall see below, the most useful production regime at a hadron collider results in relativistic  $\chi_*$  whose lifetimes in the detector frame are given by  $c\tau = \gamma c\tau_0$ , where  $\gamma = E_{\chi_*}/m_*$ . In our detailed LHC calculations below, we include this dilation factor on an event-by-event basis.

**Production of iDM particles at the LHC.** At the LHC, the interactions with quarks will result in events containing one  $\chi$  and one  $\chi_*$  in the final state. The hadrons from the  $\chi_*$  decays are generally too soft to be used as triggers. However, a “monojet” process,  $pp \rightarrow \bar{\chi}_* \chi j$  (plus the conjugate  $\bar{\chi} \chi_* j$  process) containing an additional unflavored jet  $j$  radiated from the initial partons can provide a suitable trigger. After the  $\chi_*$  decay, the final state consists of  $2\chi + j + \pi$ 's, where because of the long  $\chi_*$  lifetime, the  $\pi$ 's are produced far from the primary interaction vertex, leading to a signature of a *monojet plus displaced pions*.

Current LHC monojet searches [12, 13] rely on a missing energy trigger and apply a missing energy cut of  $\cancel{E}_T > 150$  GeV (at CMS). For the iDM signature, one may use the same triggers and missing energy cut. We simulate the expected production rate after the missing energy cut at the 7 TeV LHC using Madgraph 5 [14] with the CTEQ 6L1 [15] parton distribution functions (PDFs). The results for the various operators are shown in Fig. 2. For DM masses below around 50 GeV, the rates become independent of the value of the mass itself, because the  $\cancel{E}_T$  cut becomes the limiting factor for production.

In Fig. 3, we show the distribution of the  $\gamma$  factor for the excited WIMP (after cuts) resulting from production

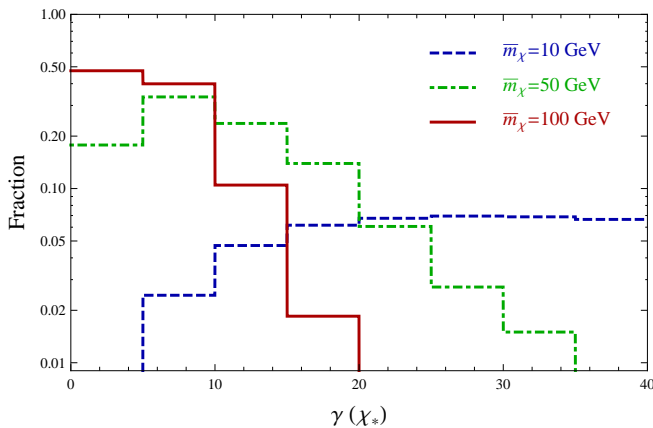


FIG. 3: The distribution of  $\gamma$  (for  $\mathcal{O}_1$ ) for three choices of DM masses after a missing energy cut of  $\cancel{E}_T \geq 150$  GeV.

through operator  $\mathcal{O}_1$ . Results from  $\mathcal{O}_{2-4}$  are very similar. As expected, the peak of the distribution shifts to larger values for smaller DM masses, and remains  $\sim 10$  for masses as large as 100 GeV. Comparing Figs. 1 and 3 reveals that for WIMP masses around 50 GeV, the lab frame decay length  $\gamma c\tau_0$  is around 1 m for a wide range of  $\Delta$  and  $\Lambda \sim 1$  TeV.

**Search strategy and discovery potential.** In addition to the primary jet against which the  $\chi\chi_*$  system recoils, iDM also produces one or more hadrons deep in the detector from the  $\chi_*$  decay. For decay lengths on scales of 10 cm to 1 m, the hadrons are likely to deposit most of their energy in the electromagnetic (ECAL) or hadronic (HCAL) calorimeters. For the discussion below, we use detailed numbers for the CMS detector [16], though similar conclusions will also hold for ATLAS. The hadrons from the  $\chi_*$  decay are not typical of QCD jets, since they contain a much smaller multiplicity of charged particles (particularly when charged pions are produced after  $\chi_*$  traverses the tracker). Aside from their relatively long decay length, these features are common between  $\chi_*$  and hadronic tau decays (the actual hadron multiplicities from  $\chi_*$  decays are different from hadronic taus and depend on the mass splitting).

For a sufficiently loose definition of a hadronic tau, the iDM decays can mimic an extra jet consistent with the hadronic tau signature. After being tagged as a hadronic tau, one can further reduce real tau backgrounds using the decay length. Our search strategy is thus a monojet together with a tau-tagged jet. At CMS, hadronic tau's resulting in visible transverse energy  $> 15$  GeV have a tagging efficiency of  $\sim 20\%$ , with a fake rate of 0.3% [17]. We adopt these numbers as estimates for the (mis)tag rates for the  $\chi_*$  decayed jet, though it would be worthwhile to have a proper treatment by the experimental collaborations using a realistic detector simulation. Given the very short  $\tau$  lifetime ( $c\tau_\tau \sim 100 \mu\text{m}$  in the  $\tau$  rest frame), we estimate that the background from  $Wj$ , where  $W \rightarrow \tau\nu$  will be essentially entirely removed

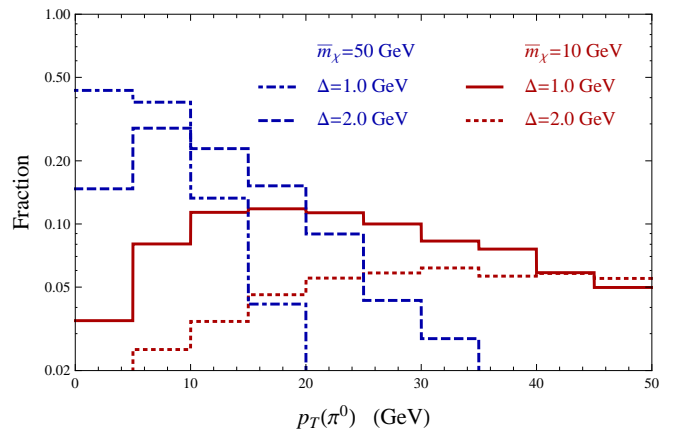


FIG. 4: The transverse energy of hadrons (resulting from operator  $\mathcal{O}_1$ ) for two choices of DM masses and splittings, as indicated.

by a displacement cut  $\gtrsim 10$  cm.

In the limit of the missing  $\cancel{E}_T > \bar{m}$  and  $\Delta \gg m_{\pi^0}$ , the total transverse energy of the displaced pions is  $p_T(\pi^0) \sim E_T \Delta / \bar{m}_\chi$ . Lighter  $\chi$  masses and larger mass splittings result in more deposited energy of displaced pions in the calorimeter. In Fig. 4 we show  $p_T$  of  $\pi^0$  (for  $\mathcal{O}_1$ ; other operators lead to similar results) for a few choices of  $\bar{m}$  and  $\Delta$ . Requiring  $p_T(\pi^0) \geq 15$  GeV, the signal efficiency drops rapidly as the mass varies from  $\bar{m} = 50$  GeV to  $\bar{m} = 10$  GeV.

In order to assess the discovery potential at the LHC, we allow for events which pass a monojet + “displaced hadronic tau” selection. Thus, we select events with:  $N_j = 2$  with  $p_T(j_1) > 110$  GeV and  $15 < p_T(j_2) < 30$  GeV as well as  $\cancel{E}_T \geq 150$  GeV. While in principle one could allow the second jet (typically from the  $\chi_*$  decay) to have a higher  $p_T$ , in practice for these choices of  $\Delta$  and  $p_T(j_1)$ , the signal is not very sensitive to the upper bound on  $p_T(j_2)$ . We require the  $\chi_*$  decay occur before the barrel ECAL, 129 cm from the center along the radial direction [16]. We apply a 20% hadronic  $\tau$ -tagging efficiency to signal events satisfying these criteria.

We take the backgrounds measured as part of the standard CMS monojet search based on  $36 \text{ pb}^{-1}$  [12] and apply the 0.3% hadronic tau mistag rate. In practice, this is an over-estimate of the background level because the presented backgrounds include both one and two jet events; however it can only over-estimate the background, and suffices for a conservative estimate of the LHC sensitivity. To estimate future reach, we rescale the background to a  $5 \text{ fb}^{-1}$  data set in order to determine the future statistical uncertainty (which is still expected to be the dominant contribution), thus determining future 95% limits on a putative signal at a 7 TeV LHC which has collected  $5 \text{ fb}^{-1}$ .

In Figs. 5 and 6 we show the expected reach in terms of the bound on the strength of the contact interaction  $\Lambda_i$  for the axial-vector interaction  $\mathcal{O}_1$  and scalar inter-

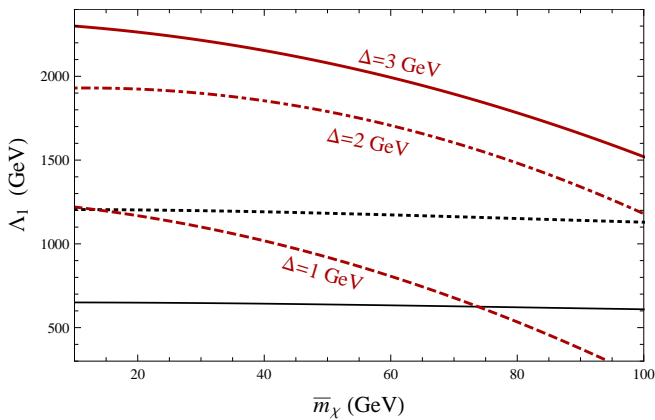


FIG. 5: The 95% C.L. exclusion limit on  $\Lambda_1$  (for  $\mathcal{O}_1$ ) as a function of  $\bar{m}$ , assuming  $5 \text{ fb}^{-1}$  of 7 TeV LHC data, for the three values of mass splitting  $\Delta$  shown. The approximately straight lines are limits derived using monojet only searches at  $36 \text{ pb}^{-1}$  (solid) and  $5 \text{ fb}^{-1}$  (dotted).

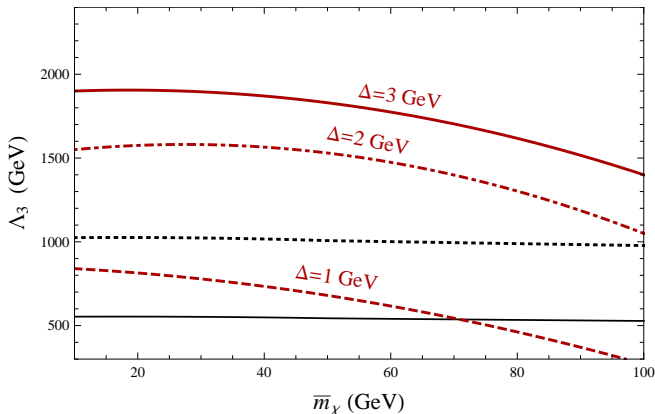


FIG. 6: The same as Fig. 5 but the scalar interaction  $\mathcal{O}_3$ .

action  $\mathcal{O}_3$ , as a function of  $\bar{m}$  and three choices of  $\Delta$ , for the LHC operating at 7 TeV and having collected  $5 \text{ fb}^{-1}$ . Also shown for reference are the limits from standard monojet searches from the existing  $36 \text{ pb}^{-1}$  and projected with  $5 \text{ fb}^{-1}$ . For mass splittings  $\gtrsim 1 \text{ GeV}$ , limits from the displaced pion search provide more stringent limits on iDM than the standard monojet search. For smaller mass splittings, the visible  $\chi_*$  decay products have difficulty passing the  $p_T \geq 15 \text{ GeV}$  cut. We find that limits on  $\mathcal{O}_1$  and  $\mathcal{O}_3$  are comparable. We expect that the vector operator  $\mathcal{O}_4$  will end up with similar prospects, whereas the pseudo-scalar  $\mathcal{O}_2$  somewhat worse prospects, because it leads to a longer  $\chi_*$  lifetime, with decays typically happening outside of the detector. In that case, the standard monojet search will probably better probe the iDM model.

**Conclusions.** In conclusion, we have examined iDM models whose larger splitting precludes their direct detection (at tree level – scattering at one loop level is nonetheless possible, but will occur with negligible rate for  $\Lambda \sim 1 \text{ TeV}$ ). We find that the LHC has the ability to search for such models for a wide variety of masses and splittings, though a novel signature involving a monojet plus extra hadrons which are reminiscent of hadronic tau decays, but appear deep in the detector. We hope these initial promising results inspire more detailed analyses by the experimental collaborations.

**Acknowledgements.** We thank G. Landsberg, M. Peskin and J. Wacker for useful discussion. Part of this work was completed at the Aspen Center for Physics, supported in part by the NSF under Grant No. 1066293. SLAC is operated by Stanford University for the US Department of Energy under contract DE-AC02-76SF00515. TMPT acknowledges the hospitality of the SLAC theory group, and is supported in part by NSF grant PHY-0970171.

- 
- [1] E. Aprile *et al.* [XENON100 Collaboration], Phys. Rev. Lett. **105**, 131302 (2010).  
[2] T. Han, R. Hempfling, Phys. Lett. **B415**, 161-169 (1997).  
[3] L. J. Hall, T. Moroi and H. Murayama, Phys. Lett. B **424**, 305 (1998).  
[4] R. Bernabei, P. Belli, F. Cappella, R. Cerulli, C. J. Dai, A. d’Angelo, H. L. He, A. Incicchitti *et al.*, Eur. Phys. J. **C67**, 39-49 (2010).  
[5] D. Tucker-Smith and N. Weiner, Phys. Rev. D **64**, 043502 (2001).  
[6] A. Birkedal, K. Matchev and M. Perelstein, Phys. Rev. D **70**, 077701 (2004); M. Beltran, D. Hooper, E. W. Kolb, Z. A. C. Krusberg and T. M. P. Tait, JHEP **1009**, 037 (2010).  
[7] J. Goodman, M. Ibe, A. Rajaraman, W. Shepherd, T. M.P. Tait and H.B. Yu, Phys. Lett. B **695**, 185 (2011); *ibid*, Phys. Rev. **D82**, 116010 (2010).  
[8] Y. Bai, P. J. Fox and R. Harnik, JHEP **1012**, 048 (2010).  
[9] A. Rajaraman, W. Shepherd, T. M.P. Tait and A.M. Wijangco, arXiv:1108.1196 [hep-ph].  
[10] P. J. Fox, R. Harnik, J. Kopp, Y. Tsai, Phys. Rev. **D84**, 014028 (2011).  
[11] M. Jamin, Phys. Lett. B **538**, 71 (2002).  
[12] S. Chatrchyan *et al.* [ CMS Collaboration ], [arXiv:1106.4775 [hep-ex]].  
[13] G. Aad *et al.* [ ATLAS Collaboration ], [arXiv:1106.5327 [hep-ex]].  
[14] J. Alwall, M. Herquet, F. Maltoni, O. Mattelaer, T. Stelzer, JHEP **1106**, 128 (2011).  
[15] J. Pumplin, D. R. Stump, J. Huston, H. L. Lai, P. M. Nadolsky, W. K. Tung, JHEP **0207**, 012 (2002).  
[16] G. L. Bayatian *et al.* [ CMS Collaboration ], “CMS physics: Technical design report,”  
[17] CMS Collaboration, CMS-PAS-TAU-11-001, 2011.